Giant galaxy growing from recycled gas: ALMA maps the circumgalactic molecular medium of the Spiderweb in [C I]

B. H. C. Emonts, M. D. Lehnert, H. Dannerbauer, C. de Breuck, M. Villar-Martín, G. K. Miley, J. R. Allison, B. Gullberg, N. A. Hatch, P. Guillard, et al.

HAL Id: insu-03747694
https://insu.hal.science/insu-03747694

Submitted on 8 Aug 2022

Giant galaxy growing from recycled gas: ALMA maps the circumgalactic molecular medium of the Spiderweb in [C I]

B. H. C. Emonts,[1]★ M. D. Lehnert,[2] H. Dannerbauer,[3,4] C. De Breuck,[5]
M. Villar-Martín,[6] G. K. Miley,[7] J. R. Allison,[8,9] B. Gullberg,[10] N. A. Hatch,[11]
P. Guillard,[2] M. Y. Mao[12] and R. P. Norris[13,14]

[1]*National Radio Astronomy Observatory, 520 Edgemont Road, Charlottesville, VA 22903, USA*
[2]*Sorbonne Université, CNRS, UMR 7095, Institut d'Astrophysique de Paris, 98bis bvd Arago, F-75014 Paris, France*
[3]*Instituto de Astrofísica de Canarias, E-38205 La Laguna, Tenerife, Spain*
[4]*Dpto. Astrofísica, Universidad de La Laguna, E-38206 La Laguna, Tenerife, Spain*
[5]*European Southern Observatory, Karl Schwarzschild Strasse 2, D-85748 Garching, Germany*
[6]*Centro de Astrobiología (INTA-CSIC), Ctra de Torrejón a Ajalvir, km 4, E-28850 Torrejón de Ardoz, Madrid, Spain*
[7]*Leiden Observatory, University of Leiden, PO Box 9513, NL-2300 RA Leiden, the Netherlands*
[8]*Sydney Institute for Astronomy, School of Physics A28, The University of Sydney, NSW 2006, Australia*
[9]*ARC Centre of Excellence for All-sky Astrophysics in 3 Dimensions (ASTRO 3D)*
[10]*Centre for Extragalactic Astronomy, Department of Physics, Durham University, Durham DH1 3LE, UK*
[11]*School of Physics and Astronomy, University of Nottingham, University Park, Nottingham NG7 2RD, UK*
[12]*Jodrell Bank Observatory, University of Manchester, Macclesfield, Cheshire SK11 9DL, UK*
[13]*CSIRO Astronomy and Space Science, Australia Telescope National Facility, PO Box 76, Epping, NSW 1710, Australia*
[14]*Western Sydney University, Penrith South, NSW 1797, Australia*

ABSTRACT

The circumgalactic medium (CGM) of the massive Spiderweb Galaxy, a conglomerate of merging proto-cluster galaxies at $z = 2.2$, forms an enriched interface where feedback and recycling act on accreted gas. This is shown by observations of [C I], CO(1-0), and CO(4-3) performed with the Atacama Large Millimeter Array and Australia Telescope Compact Array. [C I] and CO(4-3) are detected across ∼50 kpc, following the distribution of previously detected low-surface-brightness CO(1-0) across the CGM. This confirms our previous results on the presence of a cold molecular halo. The central radio galaxy MRC 1138-262 shows a very high global $L'_{CO(4-3)}/L'_{CO(1-0)} \sim 1$, suggesting that mechanisms other than FUV-heating by star formation prevail at the heart of the Spiderweb Galaxy. Contrary, the CGM has $L'_{CO(4-3)}/L'_{CO(1-0)}$ and $L'_{[CI]}/L'_{CO(1-0)}$ similar to the ISM of five galaxies in the wider proto-cluster, and its carbon abundance, $X_{[CI]}/X_{H_2}$, resembles that of the Milky Way and star-forming galaxies. The molecular CGM is thus metal-rich and not diffuse, confirming a link between the cold gas and *in situ* star formation. Thus, the Spiderweb Galaxy grows not directly through accretion of gas from the cosmic web, but from recycled gas in the CGM.

Key words: galaxies: clusters: intracluster medium – galaxies: haloes – galaxies: high-redshift – galaxies: individual: MRC1138-262 – intergalactic medium.

1 INTRODUCTION

Most of the baryons in the Universe lie outside galaxies. We can study baryonic haloes around galaxies through absorption lines towards distant quasars, or cooling radiation emitted in Lyα. Absorption-line studies detect ∼100 kpc haloes of warm, $T \sim 10^4$ K,

enriched gas around high-z galaxies and quasars (e.g. Prochaska, Lau & Hennawi 2014; Neeleman et al. 2017).

We recently discovered that the coldest gas phase can also exist in such environments, by revealing a molecular gas reservoir across the halo of the massive forming Spiderweb Galaxy at $z = 2.2$ (Emonts et al. 2016, hereafter EM16). The Spiderweb Galaxy is a conglomerate of star-forming galaxies that surround the radio galaxy MRC 1138-262, and that are embedded in a giant Lyα halo (Pentericci et al. 1997; Miley et al. 2006). We refer to the entire 200 kpc region of the Lyα halo as the 'Spiderweb Galaxy', because

★ E-mail: bjornemonts@gmail.com

it will likely evolve into a single dominant cluster galaxy (Hatch et al. 2009). The Spiderweb Galaxy is part of a larger proto-cluster (Kurk et al. 2004; Kodama et al. 2007; Dannerbauer et al. 2014).

The halo gas spans a wide range of temperatures and densities ($T \sim 100$–10^7 K, $n \sim 10^{-3}$–10^4 cm^{-3}; Carilli et al. 2002; EM16). Across the inner ~ 70 kpc, we detected $\sim 10^{11}$ M$_\odot$ of molecular gas via CO(1-0) (EM16). The location and velocity of the CO, as well as its large angular scale (EM16, their fig. S1), imply that the bulk of the molecular gas is found in the gaseous medium that lies between the brightest galaxies in the halo. We refer to this gaseous medium as the circumgalactic medium (CGM). There is also diffuse blue light across the halo, indicating that *in situ* star formation occurs within the CGM (Hatch et al. 2008). Since the surface densities of the molecular gas and the rate of star formation fall along the Schmidt–Kennicutt relation, the CO(1-0) results provided the first direct link between star formation and cold molecular gas in the CGM of a forming massive galaxy at high-z (EM16). Extended CO is also found in the CGM of a massive galaxy at $z = 3.47$ (Ginolfi et al. 2017).

Here, we present observations sensitive to low-surface-brightness extended emission of atomic carbon, [C I]^{3}P$_1$-^{3}P$_0$ (hereafter [C I]) in the CGM of the Spiderweb Galaxy. We supplement these with observations of CO(1-0) and CO(4-3) to study the chemical composition and excitation conditions of the gas. [C I] and CO(1-0) are fully concomitant in molecular clouds across the Milky Way (Ojha et al. 2001; Ikeda et al. 2002). They have a similar critical density, with the [C I] $J=1$ level well populated down to $T_k \sim 15$ K (Papadopoulos, Thi & Viti 2004). A large positive K-correction means that, at comparable resolution, [C I] is much brighter than CO(1-0). This becomes progressively more advantageous towards higher redshifts, as the instrumental $T_{\rm sys}$ at the corresponding frequencies becomes more comparable (Papadopoulos et al. 2004; Tomassetti et al. 2014). Furthermore, a high cosmic ray flux from star formation or radio jets may reduce the CO abundance in favour of [C I] (Bisbas et al. 2015, 2017).

We assume H$_0 = 71$ km s^{-1} Mpc^{-1}, $\Omega_{\rm M} = 0.27$, and $\Omega_\Lambda = 0.73$, i.e. 8.4 kpc arcsec^{-1} and $D_{\rm L} = 17\,309$ Mpc at $z = 2.2$ (EM16).

2 OBSERVATIONS

We observed the Spiderweb for 1.8 h on-source during Atacama Large Millimeter Array (ALMA) cycle-3 on 2016 January 16 in its most compact 12-m configuration (C36-1; baselines 15–161 m). We placed two adjacent spectral windows of 1.875 GHz on [C I]^{3}P$_1$-^{3}P$_0$ at $\nu_{\rm obs} \sim 155.7$ GHz ($\nu_{\rm rest} = 492.16$ GHz) and another two on CO(4-3) at $\nu_{\rm obs} \sim 145.8$ GHz ($\nu_{\rm rest} = 461.04$ GHz). The ALMA data were reduced in the Common Astronomy Software Applications (CASA) software (McMullin et al. 2007). We binned the data to 30 km s^{-1} channels and cleaned signal ≥ 1 mJy bm^{-1}. We then Hanning smoothed the data to a resolution of 60 km s^{-1}. The resulting noise is 0.085 mJy beam^{-1} channel^{-1}. We imaged our field using natural weighting out to ~ 33 arcsec, where the primary beam response drops to ~ 10 per cent sensitivity. The synthesized beam is 2.3 arcsec $\times$ 1.5 arcsec with PA $= 73.4°$.

Using the Australia Telescope Compact Array (ATCA), we made a two-pointing mosaic with an on-source time of ~ 90 h per pointing at $\nu_{\rm obs} \sim 36.5$ GHz to observe CO(1-0). The first pointing was centred on the Spiderweb Galaxy (EM16). The second one was centred ~ 23 arcsec to the west and observed in 2016 January in the 750C configuration for 42 h and in 2016 April in the H214 configuration for 40 h on-source. The observing strategy and data reduction in MIRIAD followed EM16.

Because the Spiderweb Galaxy was located near the edge of the primary beam in the second pointing, its strong continuum caused beam-smearing errors that could not be completely eliminated, even with model-based continuum subtraction in the (u,v)-domain (Allison et al. 2012). This prevented us from improving the image of the faint CO(1-0) in the halo compared with EM16. We imaged both pointings separately using natural weighting, and combined them using the task LINMOS. We binned the channels to 34 km s^{-1} and applied a Hanning smooth, resulting in a resolution of 68 km s^{-1}. The noise in the centre of the mosaic is 0.073 mJy bm^{-1}, with a beam of 4.7 arcsec $\times$ 4.1 arcsec (PA 36.3°). Velocities are in the optical frame relative to $z = 2.1612$.

3 RESULTS

Fig. 1 shows [C I], CO(4-3), and CO(1-0) from proto-cluster galaxies within a 250 kpc radius around the Spiderweb Galaxy. Six proto-cluster galaxies show line emission (Table 1).

The central radio galaxy MRC 1138-262 is covered fully by the ALMA beam and shows an extraordinary high global $L'_{\rm CO(4-3)}/L'_{\rm CO(1-0)} \sim 1$ (Table 1). In metal-rich environments, such high global gas excitation states are hard to achieve with far-UV photons from star formation, and cloud-heating mechanisms due to cosmic rays, jet-induced shocks, or gas turbulence must be prevailing (Papadopoulos et al. 2008, 2012; Ivison et al. 2012). MRC 1138-262 also has a high $L'_{\rm [CI]}/L'_{\rm CO} \sim 0.67$, exceeding that of most submm galaxies (SMGs), quasi-stellar objects (QSOs), and lensed galaxies (Walter et al. 2011; Alaghband-Zadeh et al. 2013; Bothwell et al. 2017). We compare our [C I]^{3}P$_1$-^{3}P$_0$ detection with [C I] ^{3}P$_2$-^{3}P$_1$ data from Gullberg et al. (2016), which we tapered and smoothed to the same spatial resolution (Fig. 1). We derive a [C I] fine-structure ratio of $L'_{\rm [CII]2\to 1}/L'_{\rm [CII]1\to 0} \sim 0.62$, which implies an excitation temperature $T_{\rm ex} \sim 32$ K for optically thin gas (Stutzki et al. 1997).

While the bulk of the [C I] and CO(4-3) in the Spiderweb Galaxy is associated with the central radio galaxy MRC 1138-262, we also detect emission across ~ 50 kpc in the CGM (Fig. 2). As with our previous CO(1-0) results, the extended [C I] is not co-spatial in either location or velocity with ten of the brightest satellite galaxies visible in Fig. 2 (Kuiper et al. 2011; EM16). The [C I] and CO(1-0) appear to follow the same distribution and kinematics across the velocity range where both lines are reliably detected (-87 to 273 km s^{-1} in Fig. 2). At the highest velocities, the [C I]^{3}P$_1$-^{3}P$_0$ peaks ~ 7 kpc SE of the core of the radio galaxy, at a location where previous high-resolution ALMA data found a concentration of [C I] ^{3}P$_2$-^{3}P$_1$ (Gullberg et al. 2016). The CO(4-3) and [C I] show similar morphologies.

The bright [C I] and CO(4-3) in the central ~ 2 arcsec (~ 17 kpc) beam make it non-trivial to determine flux densities across the CGM. We therefore taper the ALMA data to a beam of ~ 8 arcsec (~ 70 kpc), which covers the full CO(1-0) halo. We then take the spectrum within this tapered beam and subtract the line profile of the central radio galaxy (Fig. 1). The resulting spectra of the CGM are shown in Fig. 3. For both [C I] and CO(4-3), ~ 30 per cent of the total flux is spread on 17–70 kpc scales (Table 1). The 10 bright satellite galaxies with known redshifts, and likely also any fainter satellites (Hatch et al. 2008), do not substantially contribute to this emission. The reasons are that the galaxies have a much higher velocity dispersion than the gas (Fig. 3; Kuiper et al. 2011), and the 3σ upper limit for even the brightest satellite galaxies is $I_{\rm [CI]} < 0.028$ Jy beam^{-1} $\times$ km s^{-1} (FWHM = 200 km s^{-1}), or < 5 per cent of the [C I] brightness of the CGM.
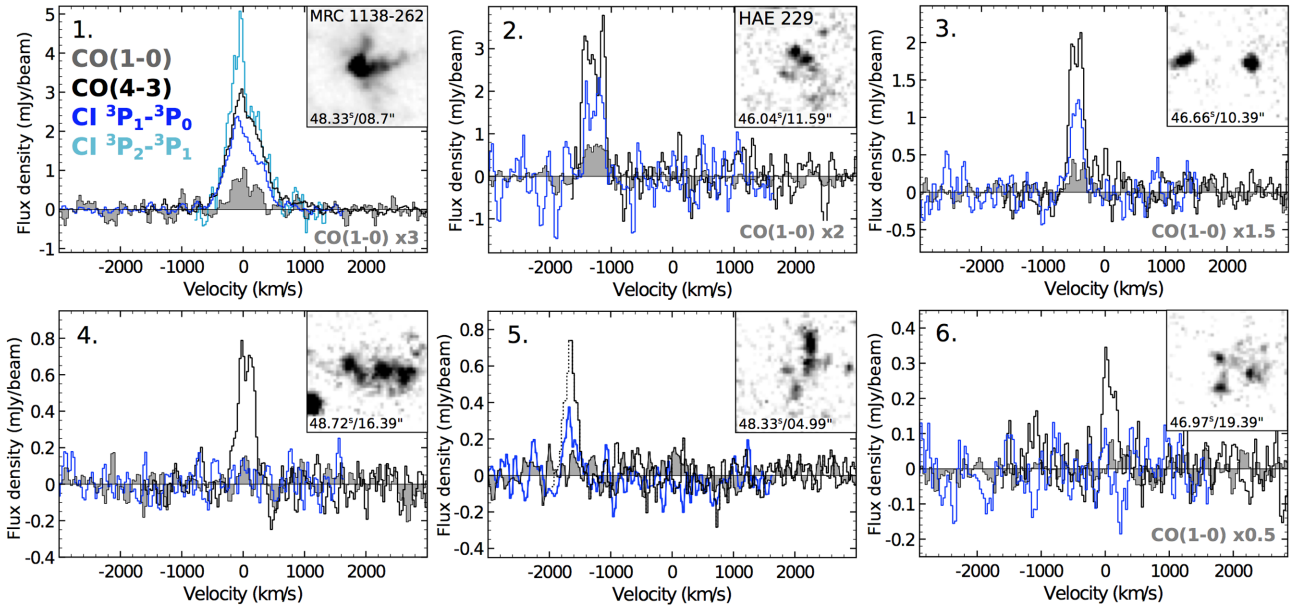
Figure 1. Spectra of [C I]^{3}P$_1$-^{3}P$_0$(blue), CO(4-3) (black), and CO(1-0) (grey) in the six proto-cluster galaxies. Except for radio galaxy MRC 1138-262, all are located far outside the Lyα halo of the Spiderweb Galaxy. Some of the CO(1-0) spectra are scaled up by a factor indicated at the bottom-right, to better visualize them. For MRC 1138-262, we also show the [C I] ^{3}P$_2$-^{3}P$_1$ line (light blue), derived by tapering and smoothing the ALMA data from Gullberg et al. (2016) to the resolution of our [C I]^{3}P$_1$-^{3}P$_0$ data. Galaxy #2 is an Hα emitter HAE 229, for which Dannerbauer et al. (2017) detected CO(1-0) across a large disc. The CO(4-3) line of galaxy #5 fell at the edge of the band, and the dotted line estimates the profile if it is symmetric. The top-right inset in each panel shows a 2 arcsec × 2 arcsec region of the galaxy in *HST*/ACS F475W+F814W imaging (Miley et al. 2006). Coordinates in seconds and arcsec are relative to RA=11^{h}40^m and δ=−26°29′.

Table 1. Emission-line properties. Velocity *v* is relative to *z* = 2.1612, while *v* and FWHM are derived by fitting a Gaussian function to the CO(4-3) line ([C I] for galaxy #5). The ratios of the brightness luminosity (*L*′) are $r_{CI/1-0} = L'_{[CI]1\to0}/L'_{CO(1-0)}$, $r_{CI/4-3} = L'_{[CI]1\to0}/L'_{CO(4-3)}$, and $r_{4-3/1-0} = L'_{CO(4-3)}/L'_{CO(1-0)}$. The molecular gas mass M_{H_2} is derived from $L'_{CO(1-0)}$ (Solomon & Vanden Bout 2005), assuming $\alpha_{CO} = M_{H_2}/L'_{CO(1-0)} = 0.8$ M$_\odot$ (K km s^{-1} pc^2)$^{-1}$ for galaxies #1–6, and $\alpha_{CO} = 4$ M$_\odot$ (K km s^{-1} pc^2)$^{-1}$ for the CGM (see EM16). The [C I] mass ($M_{[CI]}$) is estimated following Weiß et al. (2005), assuming $T_{ex} = 30$ K. Errors (in brackets) include uncertainties in *I* from both the noise (see equation 2 of Emonts et al. 2014; also Sage 1990) and the absolute flux calibration (5 per cent for ALMA; 20 per cent for ATCA).

#	v km s^{-1}	FWHM km s^{-1}	$I_{[CI]1\to0}$ Jy bm^{-1}×km s^{-1}	$I_{CO(1-0)}$	$I_{CO(4-3)}$	$r_{CI/1-0}$	$r_{CI/4-3}$	$r_{4-3/1-0}$	M_{H_2} 10^{10} M$_\odot$	$M_{[CI]}$ 10^6 M$_\odot$
1	–	610 (10)	1.32 (0.07)	0.11 (0.03)^a	1.77 (0.09)	0.66 (0.18)	0.67 (0.04)	1.00 (0.28)	2.0 (0.6)	21 (1.0)
2	−1290 (10)	375 (20)	0.60 (0.08)	0.15 (0.04)^b	1.19 (0.08)	0.22 (0.05)	0.44 (0.07)	0.49 (0.17)	2.8 (0.6)	9.5 (1.2)
3	−450 (10)	255 (15)	0.29 (0.03)	0.06 (0.02)	0.54 (0.03)	0.27 (0.09)	0.47 (0.05)	0.56 (0.19)	1.1 (0.4)	4.6 (0.5)
4	45 (10)	310 (20)	<0.03	<0.03	0.25 (0.02)	–	<0.11	>0.52	<0.6	<0.5
5	−1655 (10)	220 (15)	0.08 (0.01)	<0.03	0.16 (0.01)^c	>0.15	0.44 (0.06)	>0.33	<0.6	1.2 (0.1)
6	60 (15)	200 (25)	<0.04	<0.03	0.13 (0.02)	–	<0.27	>0.27	<0.6	<0.6
CGM	–	–	0.56 (0.09)	0.11 (0.04)	0.79 (0.07)	0.28 (0.11)	0.62 (0.11)	0.45 (0.17)	10 (4)	8.9 (1.4)

^{a}The ATCA profile in Fig. 1 provides an upper limit to the CO(1-0) content of MRC 1138-262, because the CO(1-0) data have a larger beam than the [C I] and CO(4-3) data, and therefore include more extended CO(1-0). The corresponding $I_{CO(1-0)} \lesssim 0.126$ Jy bm^{-1} × km s^{-1}. To estimate lower limit values, we tapered existing high-resolution VLA data (EM16) to the spatial resolution of our ALMA data. This gives $I_{CO(1-0)} \gtrsim 0.101$ Jy bm^{-1} × km s^{-1}. However, these VLA data have lower sensitivity, hence likely underestimate the full width of the profile. $I_{CO(1-0)}$ in the Table is a weighted average of the two values, although both values are within the uncertainties.
^{b}Dannerbauer et al. (2017) previously reported a somewhat higher $I_{CO(1-0)}$, although our estimate agrees to within the uncertainties.
^{c}CO(4-3) falls at the edge of the band and half the profile is missing. We derive values assuming that the line profile is symmetric.

4 DISCUSSION

Observations of [C I]^{3}P$_1$-^{3}P$_0$, CO(1-0), and CO(4-3) enable us to estimate the carbon abundance and excitation conditions of the molecular gas in the CGM and proto-cluster galaxies. Fig. 4 (top) shows that the values for $L'_{[CI]}/L'_{CO(4-3)}$ spread across a large range (see also Walter et al. 2011; Alaghband-Zadeh et al. 2013; Bothwell et al. 2017). When comparing the ground transitions of [C I]^{3}P$_1$-^{3}P$_0$ and CO(1-0), Fig. 4 (bottom) shows two interesting results. First, the CGM has excitation conditions, $L'_{CO(4-3)}/L'_{CO(1-0)}$, and

relative [C I] brightness, $L'_{[CI]}/L'_{CO(1-0)}$, similar to those of the proto-cluster galaxies, as well as low-*z* star-forming galaxies. Secondly, both the gas excitation and relative [C I] brightness are substantially higher in the radio galaxy MRC 1138-262. A possible explanation for the latter is that the CO(1-0) luminosity is reduced due to a high cosmic ray flux near the AGN (Bisbas et al. 2017). Alternatively, the [C I] luminosity may depend on processes that also affect the gas excitation, and thus the luminosity of high-*J* CO lines like CO(4-3) (Section 3).
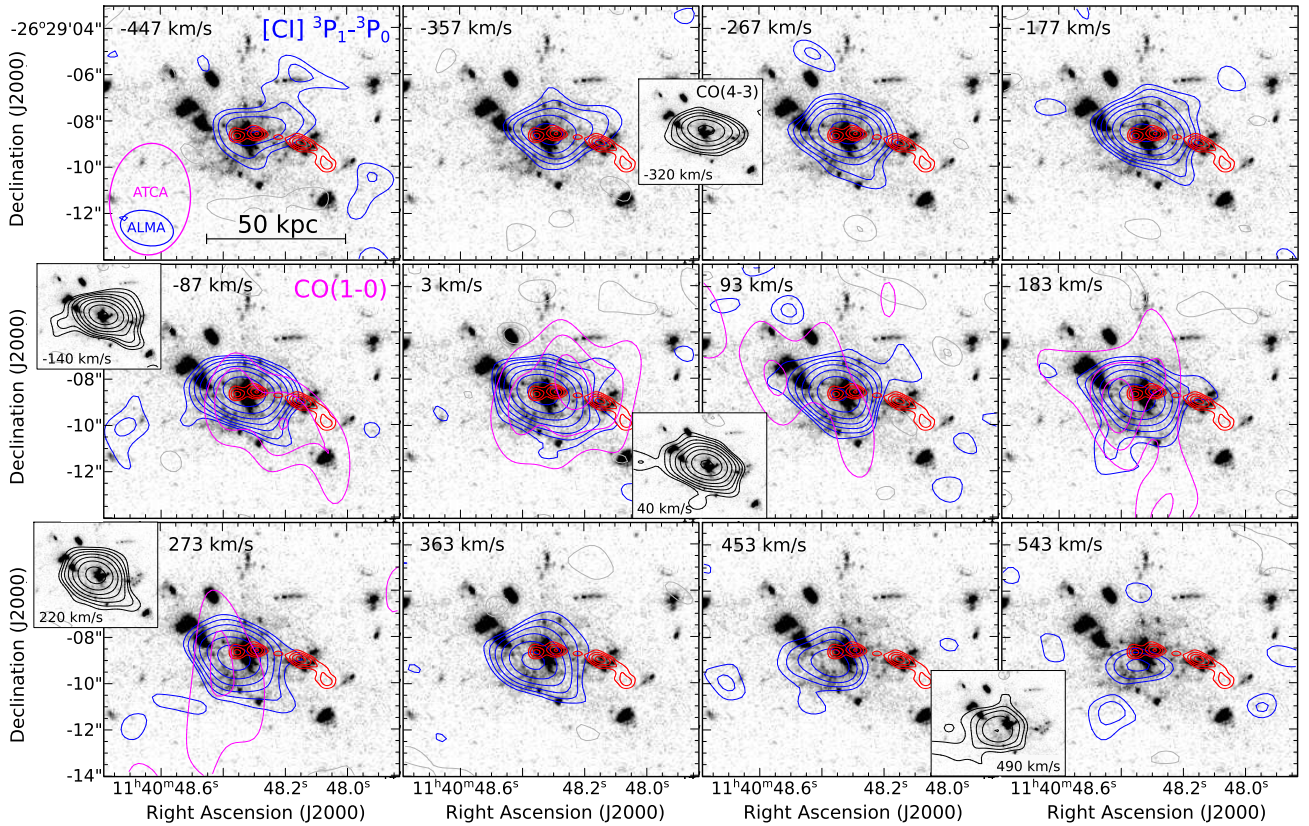
Figure 2. Channels maps of the [C I]$^3P_1$-$^3P_0$ emission (blue contours) overplotted on an *HST*/ACS F475W+F814W image of the Spiderweb Galaxy (Miley et al. 2006). The magenta contours indicate the previously detected CO(1-0) emission in channels where it is bright enough to be reliably detected (EM16). The most prominent features seen in [C I] and CO(1-0) are also detected in CO(4-3) (black contours in the insets). All data sets were binned to a velocity resolution of 90 km s^{-1}, and the central velocity of each channel is indicated. Contour levels of [C I] and CO(4-3) start at 2σ and increase by a factor of 1.5, with $\sigma = 0.07$ mJy beam^{-1} (negative contours are shown in grey). CO(1-0) contour levels are at 2σ, 3σ, 4σ, 5σ, with $\sigma = 0.086$ mJy beam^{-1}. The red contours indicate the 36-GHz radio continuum (EM16). The synthesized beams of the ALMA and ATCA data are shown in the bottom-left corner of the top-left plot.
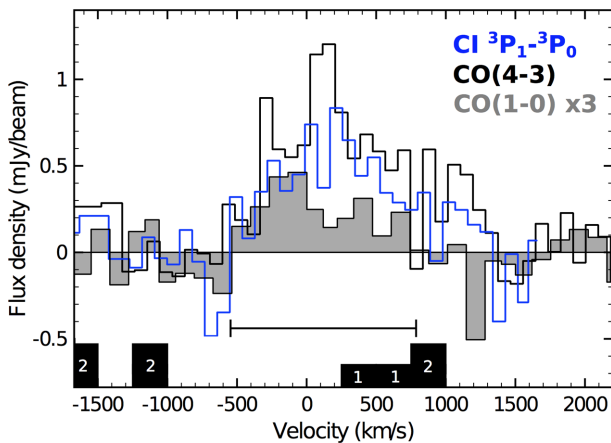

Figure 3. Emission on 17–70 kpc scales in the Spiderweb's CGM. The spectra were extracted by tapering the various data to $\sim$8 arcsec and subtracting the central 2 arcsec spectra of MRC 1138-262 (Fig. 1). For the central CO(1-0) spectrum of MRC 1138-262, we used the average between the untapered ATCA spectrum and a tapered high-resolution VLA spectrum from EM16, as explained in Table 1. The horizontal bar indicates the conservative velocity range over which we detect all three tracers in the CGM, which we used to determine intensities and ratios. The bottom histogram shows velocities of satellite galaxies that lie within the molecular halo, based on [O II], [O III], and H α (Kuiper et al. 2011).

We estimate an H$_2$ mass in the CGM on 17–70 kpc scales of $M_{H_2} \sim 1.0 \pm 0.4 \times 10^{11}(\alpha_{CO}/4)$ M$_\odot$ (Table 1; Solomon & Van den Bout 2005). The [C I] mass in the CGM is $M_{[CI]} \sim 8.9 \pm 1.4 \times 10^6$ M$_\odot$, assuming $T_{ex} \sim$30 K (Weiß et al. 2005). This results in a [C I] abundance of $X_{[CI]}/X_{H_2} = M_{[CI]}/(6M_{H_2}) \sim 1.5 \pm 0.6 \times 10^{-5}$ ($4/\alpha_{CO}$), close to that of the Milky Way ($\sim$2.2 $\times$ 10^{-5}) and other high-z star-forming galaxies (Frerking et al. 1989; Weiß et al. 2005; Bothwell et al. 2017). The H$_2$ densities must be at least $\sim$100 cm^{-3}, which is the high end of densities of the cool neutral medium, where the H I to H$_2$ transition occurs (Bialy et al. 2017). More likely, values will be close to $\sim$ 500 cm^{-3}, the critical density of [C I] (Papadopoulos et al. 2004).

4.1 Mixing in the CGM

Our findings of extended [C I], CO(1-0), and CO(4-3) imply that the cold molecular CGM is metal-rich and not diffuse. As we showed in EM16, the surface densities of the molecular CGM and the rate of *in situ* star formation across the halo fall on the same Kennicutt–Schmidt relation as for star-forming galaxies (Kennicutt 1998). The fact that the gas excitation and [C I] abundance of the CGM are similar to that of the ISM in star-forming galaxies strengthens this claim.

Despite the similarities between the CGM of the Spiderweb and the ISM in surrounding proto-cluster galaxies, it is unlikely that the cold CGM consists mainly of gas that is currently being
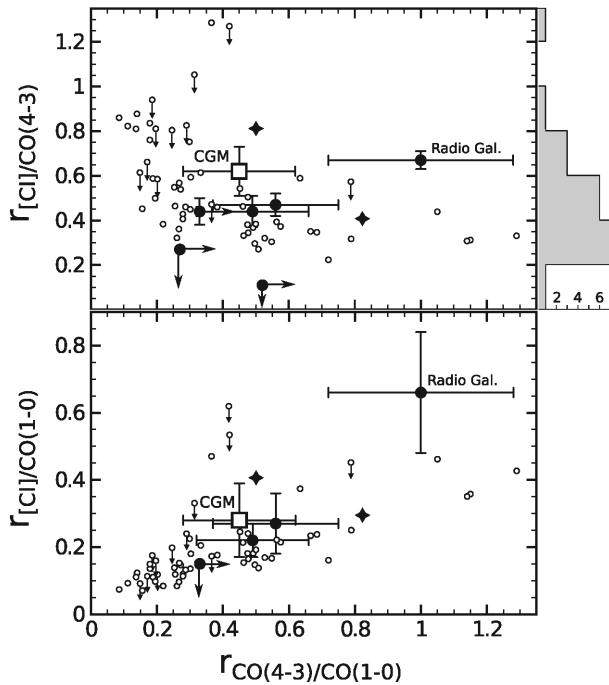
Figure 4. Ratios of the [C I], CO(1-0), and CO(4-3) lines tracing a wide range of carbon abundances and excitation conditions. The open square represents the CGM of the Spiderweb Galaxy (17–70 kpc), the large solid dots the six proto-cluster galaxies from Fig. 1. The two stars represent two high-z lensed SMGs (Lestrade et al. 2010, 2011; Danielson et al. 2011), the small open circles low-z star-forming galaxies (Israel, Rosenberg & van der Werf 2015; Rosenberg et al. 2015; Kamenetzky et al. 2016). The histogram on the right ordinate of the top panel is the $r_{CI/CO(4-3)}$ distribution of high-z SMGs and QSOs (Alaghband-Zadeh et al. 2013; Bothwell et al. 2017).

tidally stripped from proto-cluster galaxies. If originally the gas was stripped, the low velocity dispersion of the cold gas compared to that of the galaxies means that the gas must have had at least a dynamical time of $t_{dyn} \gtrsim 10^8$ yr to settle. Since the lifetime of the OB stars across the CGM is only $\sim 10^7$ yr, they must have formed long after the cold gas settled and cooled (see Hatch et al. 2008).

Our results have important implications for our understanding of galaxy formation. Most importantly, the [C I] and CO properties do not corroborate models of efficient and direct stream-fed accretion of relatively pristine gas (e.g. Dekel et al. 2009). Instead, they agree with more complex models where the gas in the CGM is a melange from various sources – metal-enriched outflows, mass transfer among galaxies, gas accretion, and mergers (Mori & Umemura 2006; Narayanan et al. 2015; Faucher-Giguère et al. 2016; Anglés-Alcázar et al. 2017). If the gas becomes multiphase and turbulent as it flows, the interaction and mixing of gas from these various sources is likely efficient (Cornuault et al. 2018). The gradual build-up of carbon, oxygen, and dust that is starting to be modelled across these extended regions mimics many of the properties that we observe in the CGM of the Spiderweb. Thus, our results support the hypothesis that galaxies grow from recycled gas in the CGM and not directly out of accreted cold gas from the cosmic web.

ACKNOWLEDGEMENTS

REFERENCES

Alaghband-Zadeh S. et al., 2013, MNRAS, 435, 1493
Allison J. R. et al., 2012, MNRAS, 423, 2601
Anglés-Alcázar D., Faucher-Giguère C.-A., Kereš D., Hopkins P. F., Quataert E., Murray N., 2017, MNRAS, 470, 4698
Bialy S., Burkhart B., Sternberg A., 2017, ApJ, 843, 92
Bisbas T. G., Papadopoulos P. P., Viti S., 2015, ApJ, 803, 37
Bisbas T. G., van Dishoeck E. F., Papadopoulos P. P., Szűcs L., Bialy S., Zhang Z.-Y., 2017, ApJ, 839, 90
Bothwell M. S. et al., 2017, MNRAS, 466, 2825
Carilli C. L., Harris D. E., Pentericci L., Röttgering H. J. A., Miley G. K., Kurk J. D., van Breugel W., 2002, ApJ, 567, 781
Cornuault N., Lehnert M. D., Boulanger F., Guillard P., 2018, A&A, 610, 75
Danielson A. L. R. et al., 2011, MNRAS, 410, 1687
Dannerbauer H. et al., 2014, A&A, 570, A55
Dannerbauer H. et al., 2017, A&A, 608, A48
Dekel A. et al., 2009, Nature, 457, 451
Emonts B. H. C. et al., 2014, MNRAS, 438, 2898
Emonts B. H. C. et al., 2016, Science, 354, 1128
Faucher-Giguère C.-A., Feldmann R., Quataert E., Kereš D., Hopkins P. F., Murray N., 2016, MNRAS, 461, L32
Frerking M. A., Keene J., Blake G. A., Phillips T. G., 1989, ApJ, 344, 311
Ginolfi M. et al., 2017, MNRAS, 468, 3468
Gullberg B. et al., 2016, A&A, 591, 73
Hatch N. A., Overzier R. A., Röttgering H. J. A., Kurk J. D., Miley G. K., 2008, MNRAS, 383, 931
Hatch N. A., Overzier R. A., Kurk J. D., Miley G. K., Röttgering H. J. A., Zirm A. W., 2009, MNRAS, 395, 114
Ikeda M., Oka T., Tatematsu K., Sekimoto Y., Yamamoto S., 2002, ApJS, 139, 467
Israel, F., Rosenberg, M., van der Werf, P., 2015, A&A, 578, 95
Ivison R. J. et al., 2012, MNRAS, 425, 1320
Kamenetzky J., Rangwala N., Glenn J., Maloney P. R., Conley A., 2016, ApJ, 829, 93
Kennicutt Jr, R. C., 1998, ApJ, 498, 541
Kodama T., Tanaka I., Kajisawa M., Kurk J., Venemans B., De Breuck C., Vernet J., Lidman C., 2007, MNRAS, 377, 1717
Kuiper E. et al., 2011, MNRAS, 415, 2245
Kurk J. D., Pentericci L., Overzier R. A., Röttgering H. J. A., Miley G. K., 2004, A&A, 428, 817
Lestrade J.-F., Combes F., Salomé P., Omont A., Bertoldi F., André P., Schneider N., 2010, A&A, 522, L4
Lestrade J.-F., Carilli C. L., Thanjavur K., Kneib J.-P., Riechers D. A., Bertoldi F., Walter F., Omont A., 2011, ApJ, 739, L30
McMullin J. P., Waters B., Schiebel D., Young W., Golap K., 2007, in Richard A. S., Frank H., David J. B., eds, ASP Conf. Ser. Vol. 376, Astronomical Data Analysis Software and Systems XVI. Astron. Soc. Pac., San Francisco, p. 127

Miley G. K. et al., 2006, ApJ, 650, L29

Mori M., Umemura M., 2006, Nature, 440, 644

Narayanan D. et al., 2015, Nature, 525, 496

Neeleman M., Kanekar N., Prochaska J. X., Rafelski M., Carilli C. L., Wolfe A. M., 2017, Science, 355, 1285

Ojha R. et al., 2001, ApJ, 548, 253

Papadopoulos P., Thi W., Viti S., 2004, MNRAS, 351, 147

Papadopoulos P. P., Kovacs A., Evans A. S., Barthel P., 2008, A&A, 491, 483

Papadopoulos P. P., van der Werf P. P., Xilouris E. M., Isaak K. G., Gao Y., Mühle S., 2012, MNRAS, 426, 2601

Pentericci L., Roettgering H. J. A., Miley G. K., Carilli C. L., McCarthy P., 1997, A&A, 326, 580

Prochaska J. X., Lau M., Hennawi J., 2014, ApJ, 796, 140

Rosenberg M. J. F. et al., 2015, ApJ, 801, 72

Sage L. J., 1990, A&A, 239, 125

Solomon P. M., Vanden Bout P. A., 2005, ARA&A, 43, 677

Stutzki J. et al., 1997, ApJ, 477, L33

Tomassetti M., Porciani C., Romano-Díaz E., Ludlow A. D., Papadopoulos P. P., 2014, MNRAS, 445, L124

Walter F., Weiß A., Downes D., Decarli R., Henkel C., 2011, ApJ, 730, 18

Weiß A., Downes D., Henkel C., Walter F., 2005, A&A, 429, 25

This paper has been typeset from a TeX/LaTeX file prepared by the author.